An Accelerated State of Myosin-Based Actin Motility†

Anneka M. Hooft,‡ Erik J. Maki,‡ Kristine K. Cox, and Josh E. Baker*

Department of Biochemistry, University of Nevada, Reno, School of Medicine, Reno, Nevada 89557

Received July 21, 2006; Revised Manuscript Received December 29, 2006

ABSTRACT: We use an in vitro motility assay to determine the biochemical basis for a hypermotile state of myosin-based actin sliding. It is widely assumed that the sole biochemical determinant of actin-sliding velocities, *V*, is actin−myosin detachment kinetics ($1/\tau_{on}$), yet we recently reported that, above a critical ATP concentration of ∼100 μM, *V* exceeds the detachment limit by more than 2-fold. To determine the biochemical basis for this hypermotile state, we measure the effects of ATP and inorganic phosphate, P_i, on *V* and observe that at low [ATP] *V* decreases as ln [P_i], whereas above 100 μM ATP the hypermotile *V* is independent of P_i. The ln [P_i] dependence of *V* at low [ATP] is consistent with a macroscopic model of muscle shortening, similar to Hill's contractile component, which predicts that *V* varies linearly with an internal force (Hill's active state) that drives actin movement against the viscous drag of myosin heads strongly bound to actin (Hill's dashpot). At high [ATP], we suggest that the hypermotile *V* is caused by shear thinning of the resistive population of strongly bound myosin heads. Our data and analysis indicate that, in addition to contributions from τ_{on} and myosin's step size, *d*, *V* is influenced by the biochemistry of myosin's working step as well as resistive properties of actin and myosin.

Muscle contracts when the thousands of myosin molecules contained within repeatedly interact with actin filaments through a reaction cycle (Figure 1) fueled by ATP hydrolysis (*1*−*4*). A single myosin head generates force and actin filament movement with a large and discrete segmental rotation induced by strong actin binding and associated with P_i release (*5*−*11*). Here we refer to this transition as myosin's working step (the M·D·P_i to A·M·D transition in Figure 1). In contrast to this single molecule mechanism, when a collection of myosin molecules moves an actin filament in muscle or in an in vitro motility assay (*12*, *13*), the actin-sliding velocity is influenced significantly by actin−myosin detachment kinetics, $1/\tau_{on}$ (*14*−*16*). This is because when many myosin heads interact with an actin filament, a small fraction of heads is always bound to actin in the A·M·D or A·M states (Figure 1) resisting actin movement. The faster these heads dissociate from actin, the faster actin is allowed to move.

Beyond simply influencing *V*, however, it is widely held that detachment kinetics ($1/\tau_{on}$) fully limits actin movement (*17*−*19*). According to this detachment-limited model, actin movement is fully attenuated by actin-bound myosin heads, and thus sliding velocities are thought to follow the relationship $V = d/\tau_{on}$, where the myosin step size, *d*, is the distance that a single myosin head moves an actin filament and the attachment lifetime, τ_{on}, is the average time myosin spends strongly bound to actin in the A·M·D or A·M states (Figure 1). While the influence of detachment kinetics on *V* is not disputed, it remains unclear whether detachment kinetics is the sole biochemical determinant of *V*. In fact, the detachment-limited view that compliant cross-bridges between two surfaces fully attenuate the sliding of those two surfaces runs counter to our molecular understanding of viscosity (*20*). In contrast to the detachment-limited model, a macroscopic (thermodynamic, collective, or ensemble) model of muscle contraction has been proposed (*21*−*23*) that resembles Hill's contractile component (*24*) and predicts that *V* is influenced by the force-generating biochemistry of myosin's working step. According to this model, *V* is damped but not fully attenuated by attached cross-bridges, and thus *V* is not completely limited by detachment kinetics.

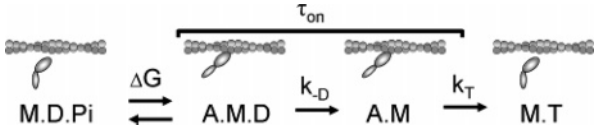

FIGURE 1: A minimal scheme for the actin−myosin ATPase reaction cycle. Myosin (M, ovals) undergoes a segmental rotation upon strong binding to actin (A, helical structure) and inorganic phosphate (P_i) release. We refer to this transition (M·D·P_i to A·M·D) as myosin's working step or the weak-to-strong binding transition. Myosin then releases ADP (A·M·D to A·M) and then binds ATP (A·M to M·T) before dissociating from actin. Finally, ATP is hydrolyzed, and the products ADP and P_i remain bound to myosin, bringing myosin back to the M·D·P_i state.

Recent studies provide support for this model. Sweeney and co-workers showed that, among different myosin isoforms and mutations, detachment kinetics is not the sole biochemical determinant of actin-sliding velocities (*25*). Additional support comes from recent studies demonstrating a shift in the [ATP] dependence of *V*, with *V* exceeding the detachment limit by more than 2-fold above a critical ATP concentration of ∼100 μM (*26*).

In this paper, to determine whether attachment kinetics contributes to the enhanced velocities observed at high

† This work was supported by a National Institutes of Health grant (P20RR018751-03 to J.E.B.). J.E.B. was funded through National Center for Research Resources Grant 5P20RR018751-02.

* To whom correspondence should be addressed. Tel: 775-784-4103. Fax: 775-784-1419. E-mail: jebaker@unr.edu.

‡ Authors contributed equally.

10.1021/bi0614840 CCC: $37.00
Published on Web 02/16/2007

physiological [ATP], we determine the biochemical basis for the observed break in the [ATP] dependence of *V*. We show that both whole myosin and myosin subfragment (S1) exhibit a similar shift in the [ATP] dependence of *V*, indicating that this phenomenon is not caused by cooperativity between the two heads of a myosin molecule. We also observe that temperature has a differential effect on velocities measured above and below the break point, suggesting that the shift in [ATP] dependence is caused by a change in the biochemistry of actin sliding. Finally, we show that below ~100 μM ATP *V* decreases as ln [P_i], whereas above ~100 μM ATP *V* is unaffected by P_i, implying that the biochemistry underlying *V* shifts from P_i-dependent to P_i-independent above the critical [ATP]. The ln [P_i] dependence of *V* observed at low [ATP] indicates that *V* is influenced by the free energy, ΔG, for myosin's force-generating transition. We show that this is consistent with Hill's proposal that shortening muscle generates a maximal internal force (active state) against a viscous drag (dashpot). The lack of a P_i effect at high ATP indicates that the internal force is dissipated, presumably through shear thinning of actin-bound myosin heads. We argue that this is the mechanism for the hypermotile *V*.

Changes in muscle shortening velocities observed with changes in cellular milieu, muscle fatigue, aging, myosin isoform shifts, disease-related mutations, etc. are routinely interpreted in terms of changes in only two parameters: *d* and τ_{on}. Our data and analysis suggest a new set of potential variables. In addition to the contributions of *d* and τ_{on}, *V* can be influenced both by the biochemistry of myosin's working step and by the resistive properties of actin and myosin.

EXPERIMENTAL PROCEDURES

Protein Purification. Fast skeletal muscle myosin was prepared from chicken pectoralis as previously described (*27*) and stored in glycerol at −20 °C. Myosin subfragment 1 (S1) was prepared from papain digestion of skeletal myosin. Actin was isolated from chicken pectoralis (*28*) and stored on ice at 4 °C. For in vitro motility assays, actin was incubated with tetramethylrhodamine isothiocyanate (TRITC) phalloidin overnight.

Buffers. For the actin-based motility assay, myosin buffer (300 mM KCl, 25 mM imidazole, 1 mM EGTA,[1] 4 mM $MgCl_2$, 10 mM DTT), actin buffer (25 mM KCl, 25 mM imidazole, 1 mM EGTA, 4 mM $MgCl_2$, 10 mM DTT), and motility buffer (25 mM KCl, 25 mM imidazole, 1 mM EGTA, 4 mM $MgCl_2$, 10 mM DTT, 0.07−1 mM ATP, 0−40 mM P_i, 0.5% methylcellulose) were used. For our 40 mM P_i experiments, P_i was added to motility buffer containing no KCl. For the corresponding zero P_i control experiments, the ionic strength was maintained by adding KCl to the motility buffer (*29*). Motility buffers with intermediate P_i concentrations were created using a mixture of the zero KCl and zero P_i buffers to maintain the ionic strength as previously described (*21*).

Activity Assays. The velocity of fluorescently labeled actin filaments sliding over a bed of myosin molecules was measured using an in vitro motility assay at 30 °C. Flow cells were prepared by attaching a nitrocellulose-coated coverslip to a microscope slide with shim spacers. Flow cells for the motility assay were prepared as follows: 2 × 40 μL washes of 100 μg/mL myosin with a 1 min incubation period, 2 × 40 μL washes with 0.5 mg/mL BSA, 2 × 40 μL washes of 10 mM actin with a 1 min incubation period, 2 × 40 μL washes with actin buffer, and 2 × 40 μL washes with motility buffer. Experiments were performed with myosin preparations that were less than 2 months old. With these preparations we found little, if any, effect of purification of "dead head" myosin through actin spin down or actin blocking protocols, indicating that actin motility was unaffected by dead heads; thus in these experiments we did not further purify dead heads prior to our experiments. Motility assays were performed using a Nikon TE2000 epifluorescence microscope with fluorescent images digitally acquired with a Roper Cascade 512B (Princeton Instruments, Trenton, NJ) camera. For each flow cell, we recorded three 30 s image sequences from three different fields, each containing approximately 10−15 actin filaments. Data obtained from these three fields constitutes one ($n = 1$) experiment. For each image sequence, we analyzed actin movement using Simple PCI tracking software (Compix, Sewickley, PA) to obtain actin-sliding velocities, *V*. Objects were defined by applying an exclusionary area threshold to minimize background noise. Intersect filters were applied to exclude intersecting filaments. The velocities of the moving actin filaments were plotted as a histogram and fitted to a Gaussian distribution. The average velocity, *V*, for the field was taken from the mean of the Gaussian fit. Velocities obtained from the Gaussian distributions of the three image fields per flow cell were used to calculate an average velocity for the flow cell. These experiments were repeated at least three times for each condition.

Kinetic and Energetic Modeling. According to a thermodynamic muscle model, muscle contraction is more accurately described by tracking the flow of macroscopic energy in the system than by tracking artificially constrained molecular mechanics. The flow of energy can be quantitatively described using nonequilibrium steady-state thermodynamics, and from this energetic analysis we obtain a formal relationship between muscle force, muscle shortening velocities, and actin−myosin biochemistry. A thermodynamic muscle model has been used to accurately describe the relationship between isometric muscle force, F_0, temperature, [ADP], [ATP], and [P_i] (*22*), and directly accounts for the observation (*21*, *30*) that changes in temperature and [P_i] affect F_0 without affecting the number of myosins bound to actin.

According to nonequilibrium steady-state thermodynamics, the free energy for the actin−myosin strong binding transition, ΔG, is transferred to work, *w*, and heat, *q*, at the rate of ATP turnover, *v*. In other words, $v\Delta G = dq/dt + dw/dt$, where the power output, dw/dt, with the weak-to-strong binding transition is *FV* and heat dissipated through resistive heads, dq/dt, is $F_{res}V$. Here *F* is the force against which muscle shortens and F_{res} is a drag force exerted by a resistive population of actin-attached myosin heads. F_{res} can be written as $F_{res} = nF_{resuni}\tau_{on}/\tau_{cycle}$, where F_{resuni} is the average drag force per attached myosin head and $n\tau_{on}/\tau_{cycle}$ is the number

[1] Abbreviations: BDM, 2,3-butanedione monoxime; EGTA, ethylene glycol bis(β-aminoethyl ether)-*N*,*N*,*N*′,*N*′-tetraacetic acid; DTT, dithiothreitol.

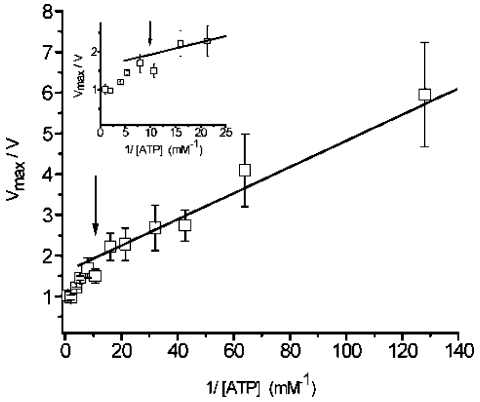

FIGURE 2: ATP dependence of actin-sliding velocities (V). Velocities were measured at ATP concentrations ranging from 0.007 to 1 mM and plotted in a double reciprocal plot. V_{max} is 2.33 μm·s^{-1}, and the solid line is a least-squares fit of a detachment limited model for velocity, $1/V = \tau_{on}/d = 1/(dk_{-D}) + 1/(dk_T[ATP])$ (*26*), giving values for an ADP release rate, k_{-D}, of 130 s^{-1} and a second-order ATP binding constant, k_T, of 6.5×10^6 M^{-1} s^{-1}. These are similar to previously reported values (*26*). The arrow indicates the critical ATP concentration (100 μM) above which velocities exceed the detachment limit, $V = d/\tau_{on}$.

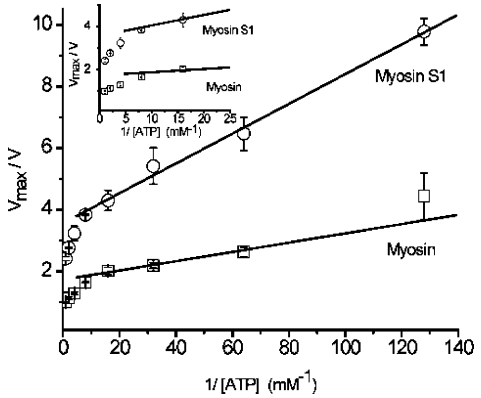

FIGURE 3: ATP dependence of actin-sliding velocities for both one- (S1) and two-headed myosin. Velocities were obtained for both single-headed myosin subfragment 1 (S1) and double-headed muscle myosin and then plotted in a double reciprocal plot. These data show that both two-headed and one-headed myosin exhibit the same hypermotile state above a similar critical ATP concentration of ~100 μM, indicating that the enhancement of V above 100 μM ATP does not result from an enhancement of step size due to head−head cooperativity.

of actin-attached myosin heads out of a total of n myosin heads. Similarly, the ATPase rate, υ, can be written as $\upsilon = n/\tau_{cycle}$, where τ_{cycle} is the average time it takes one myosin head to complete one ATP hydrolysis cycle. Thus for unloaded ($F = 0$) muscle shortening, actin-sliding velocities in an in vitro assay can be expressed as $V = \Delta G/(F_{resuni}\tau_{on})$. According to this model (*22*), $\Delta G = F_0 d$, where F_0 is active isometric muscle force and d is myosin's step size. And so we can write

$$V = \Delta G/(F_{resuni}\tau_{on}) = F_0 d/(F_{resuni}\tau_{on}) \qquad (1)$$

RESULTS

We previously reported that above a critical ATP concentration of ~100 μM a hypermotile state of myosin-based actin motility is observed for both smooth and skeletal (*26*, *31*) muscle myosin. Here we repeat these experiments using an in vitro motility assay to measure actin-sliding velocities generated by skeletal muscle myosin molecules at ATP concentrations ranging from 0.007 to 1.0 mM. In Figure 2 we present our results in a double reciprocal plot. According to a detachment-limited model of actin-sliding velocities ($V = d/(1/k_T[ATP] + 1/k_{-D})$, the data in Figure 2 should follow a linear relationship with a slope of $1/k_T$, where k_T is the second-order ATP-induced dissociation rate constant, and a y-intercept of $1/k_{-D}$, where k_{-D} is the ADP release rate (*26*). The observed break in this linear relationship (Figure 2) indicates that the biochemistry underlying V shifts at a critical ATP concentration of 100 μM. This phenomenon is most easily identified and analyzed using double reciprocal plots (*26*). As previously reported (*26*), at low [ATP] actin-sliding velocities vary linearly with $1/\tau_{on}$ values measured in a laser trap, consistent with the conventional detachment-limited model ($V = d/\tau_{on}$). However, at ATP concentrations above ~100 μM, actin-sliding velocities exceed the detachment limit, approaching a velocity more than 2-fold greater than d/τ_{on} at saturating (>1 mM) [ATP] (*26*). The molecular basis for this hypermotile state remains unknown.

One possible interpretation is that the accelerated motile state results from cooperativity between the two heads of a myosin molecule. Here we consider the possibility that the 2-fold enhancement of V at high ATP is related to the 2-fold difference in myosin's step size, d, observed between single-headed myosin subfragment 1 and double-headed myosin (*32*). To test this hypothesis, we measure actin-sliding velocities at different ATP concentrations for both whole skeletal muscle myosin and myosin subfragment 1 (S1). Figure 3 shows that both myosin and myosin S1 exhibit a similar enhancement in V above a critical ATP concentration of ~100 μM, indicating that the mechanism by which V is accelerated does not involve cooperativity between the two heads of a myosin molecule.

The observed shift in the [ATP] dependence of V appears to be caused by a change in the biochemistry of actin movement. To further test this hypothesis, we measure the effects of temperature on the [ATP] dependence of V (Figure 4). According to a detachment-limited model of actin sliding ($V = d/\tau_{on}$) the slope of the double reciprocal plot in Figure 4 is equal to $1/(dk_T)$, and the y-intercept is $1/(dk_{-D})$, where k_T is the second-order ATP-induced actin−myosin dissociation rate and k_{-D} is the ADP release rate. From a least-squares linear fit of both high and low [ATP] data in Figure 4, we determined the kinetic rate constants k_T and k_{-D} and plotted them in panels B and C of Figure 4, respectively. For these fits we used a value for d of 10 nm, which is at the upper end of the 5−10 nm range of measured step sizes (*5*, *6*). Using a value for d of 5 nm results in a 2-fold increase in estimates for k_T and k_{-D}. These data show that estimates for k_T and k_{-D} as well as their temperature dependencies differ at high versus low [ATP], further implying that the biochemistry underlying V shifts at the critical [ATP]. The experiments below indicate that this shift reflects a change in the mechanism of motility (i.e., a change in the model required for estimating k_T and k_{-D}) rather than an actual change in k_T or k_{-D}.

To establish the biochemical basis for this change in the actin-sliding biochemistry, we measure the effects of inor-

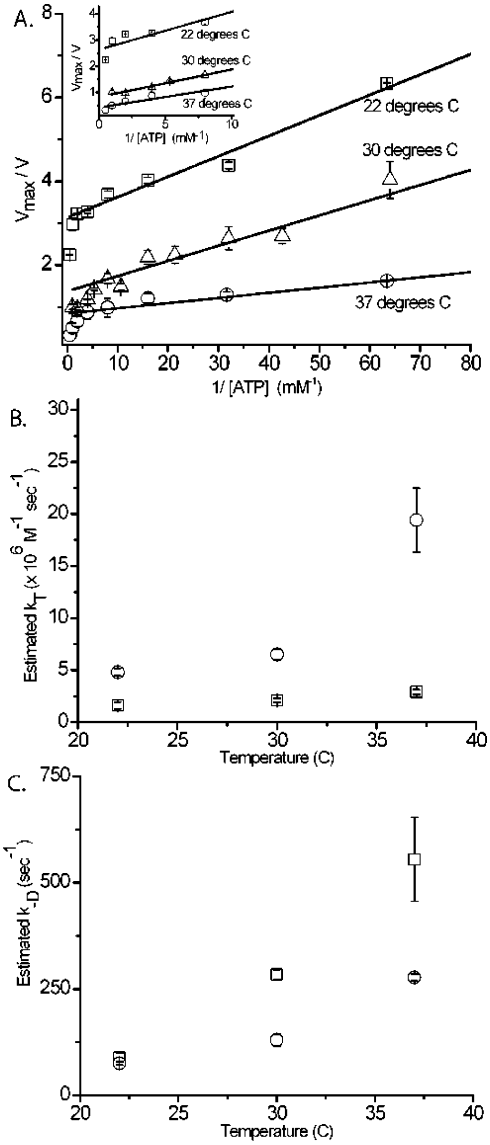

FIGURE 4: Temperature dependence of actin-sliding velocities. (A) Velocities were measured over a wide range of ATP concentrations at 22, 30, and 37 °C and plotted in a double reciprocal plot. Error bars are SEM. Using a detachment-limited model ($V = d/\tau_{on}$), where $\tau_{on} = 1/(k_T[ATP]) + 1/k_{-D}$ (*26*), we fitted both high and low [ATP] data to a line, obtaining values for $k_{-D} = 1/(d \times \text{int})$ and $k_T = 1/(d \times \text{slope})$ from the *y*-intercepts (int) and slopes with $d = 10$ nm. (B) Values for k_{-D} obtained from both high (squares) and low (circles) [ATP] data were plotted at three different temperatures. (C) Values for k_T obtained from both high (squares) and low (circles) [ATP] data were plotted at three different temperatures.

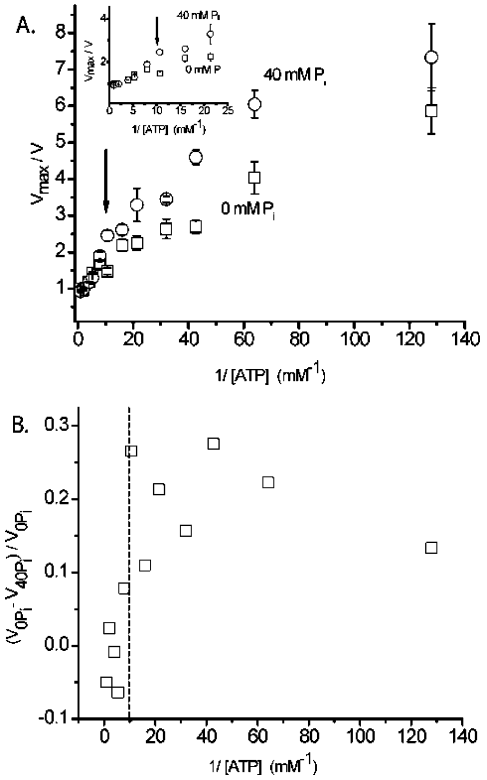

FIGURE 5: ATP dependence of *V* both with and without 40 mM added inorganic phosphate (P_i). (A) Velocities measured over a wide range of ATP concentrations both with (open circles) and without (open squares) 40 mM added P_i are plotted in a double reciprocal plot. Error bars are SEM. These data show that P_i affects *V* below but not above the critical ATP concentration (arrow), indicating that the acceleration of *V* above the critical ATP concentration involves a transition from P_i-dependent to P_i-independent actin-sliding biochemistry. (B) The fractional decrease in velocity upon addition of 40 mM P_i over a range of [ATP] was calculated from the data in Figure 4A as [(velocity with no added P_i) − (velocity with 40 mM added P_i)]/(velocity with no added P_i). These data are plotted at different ATP concentrations and show a dramatic shift in P_i sensitivity at the critical ATP concentration (dashed line).

ganic phosphate, P_i, on *V* both above and below the critical ATP concentration. Figure 5A is a double reciprocal plot of actin-sliding velocities measured at ATP concentrations ranging from 0.007 to 1.0 mM both in the presence and in the absence of 40 mM added inorganic phosphate. These data show that P_i affects actin-sliding velocities below but not above the critical ATP concentration, implying that the change in the [ATP] dependence of *V* involves a shift from P_i-dependent to P_i-independent biochemistry.

The effects of P_i on actin-sliding velocities observed at low ATP concentrations have been previously reported and interpreted as P_i inhibition of detachment kinetics. Specifically, it has been suggested that P_i competes with ATP for the no-nucleotide, rigor (A·M) heads (*33*−*35*). However, this interpretation does not account for the rather dramatic decrease in the P_i sensitivity of *V* observed above the critical ATP concentration (Figure 5B). An alternative interpretation is provided by a macroscopic (thermodynamic) model of muscle contraction (*22*). This model predicts that P_i inhibits *V* through its effect on the free energy, ΔG, for actin−myosin strong binding (eq 1), which varies as ln [P_i] (Figure 1). This model is the molecular equivalent of Hill's contractile component, in which *V* varies linearly with muscle's maximum force, which has a ln [P_i] dependence (*33*).

The above interpretations for the P_i dependence of *V* are testable. If P_i competitively inhibits *V*, we would expect *V* to vary as a parabolic function of [P_i], whereas if P_i affects *V* through a change in ΔG, we would expect *V* to decrease logarithmically with [P_i] much like isometric muscle force (*33*). Using an in vitro motility assay, we measure actin-sliding velocities at P_i concentrations ranging from 0 to 24 mM at both 10 and 20 μM ATP. These data are plotted in Figure 6 and show that *V* decreases as ln [P_i], supporting a thermodynamic model of actin sliding at low [ATP]. Indeed, the data in Figure 6 are accurately described by eq 1, with the free energy for the weak-to-strong actin−myosin binding

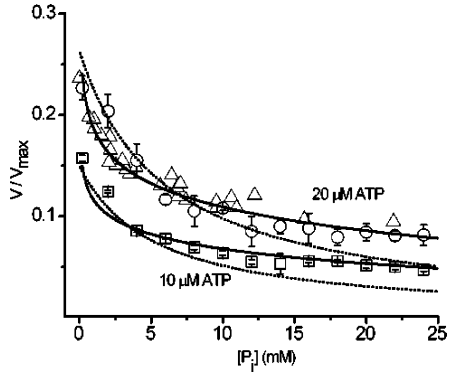

FIGURE 6: P_i dependence of V at two different ATP concentrations. Actin-sliding velocities (V) were measured at P_i concentrations ranging from 0 to 24 mM at both 10 (squares) and 20 (circles) μM ATP and plotted. The data are accurately fitted to eq 1, which takes the general form $V/V_{max} = (B - A \ln [P_i])/\{1/(k_T[ATP]) + 1/k_{-D}\}$ after making the experimentally and theoretically justified substitutions $F_0 = b - a \ln [P_i]$ and $\tau_{on} = 1/k_T[ATP] + 1/k_{-D}$, where a and b are constants (*21*, *22*, *38*). Solid lines are a global fit of this equation to data obtained at both 10 and 20 μM ATP, with $A = 0.003$ μm, $B = 5.4 \times 10^{-4}$ μm, $k_{-D} = 125$ s^{-1}, and $k_T = 7 \times 10^6$ M^{-1} s^{-1}. The dashed lines are a global fit of the same two data sets to a model of competitive inhibition by P_i, $V = [ATP]/\{[ATP] + K_M(1 + [P_i]/K_I)\}$, with $K_M = 0.055$ mM, $K_I = 6.5$ mM, and $V_{max} = 2.3$ μm s^{-1}. Here K_M is the [ATP] at half-maximal V, and K_I is the P_i inhibition constant (*35*). These data and fits indicate that the P_i dependence of V is most accurately described by a macroscopic model of muscle contraction (eq 1). Interestingly, these V data are similar to the P_i dependence of muscle force, F_0 (triangles), previously reported by Pate, Cooke, and others (*33*, *34*). Values for isometric muscle force are plotted with arbitrary units and are intended to show that both F_0 and V exhibit a similar ln $[P_i]$ dependence.

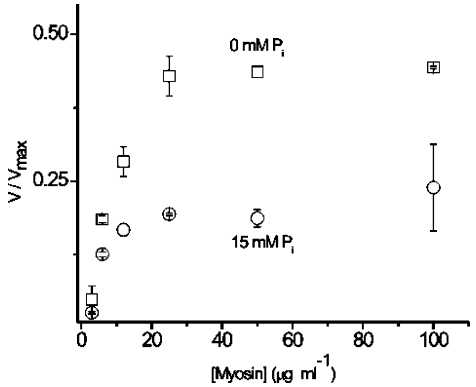

FIGURE 7: Myosin surface density dependence of V at low [ATP] and high $[P_i]$. Actin-sliding velocities, V, were measured at different myosin surface densities in the presence of 20 μM ATP and 15 mM P_i. The surface density was adjusted by varying the concentration of myosin used to incubate the flow cell over a range from 15 to 100 μg/mL (*37*). The data clearly show that both with and without added P_i, V saturates at myosin densities achieved by incubating flow cells with 30 μg/mL myosin. Because all other experiments presented in this paper were performed by incubating flow cells with 100 μg/mL myosin, these data indicate that the mechanism by which P_i slows V does not involve a significant change in the duty ratio through shifting myosin from attached to detached states.

transition, ΔG, varying as ln $[P_i]$ (see Figure 6 legend). Also predicted by eq 1, Figure 6 shows that the P_i dependence of V is remarkably similar to the P_i dependence of active, isometric muscle force, F_0.

It is plausible that phosphate's effect on V results from a change in the actin−myosin duty ratio (*36*), caused by a P_i-induced redistribution of myosin heads from A·M·D to M·D·P_i. The duty ratio is the fraction of time a myosin head spends moving an actin filament. Thus a P_i-induced decrease in duty ratio might render the myosin density used in the above experiments subsaturating for V, leading to a lower V. To determine whether V is saturated by the myosin surface densities used in the above studies, we use an in vitro motility assay to measure V at different myosin surface densities (*36*, *37*). Figure 7 shows that, at 20 μM ATP, actin-sliding velocities saturate at myosin densities approximately 3-fold lower than the densities used in the above studies independent of P_i concentration, indicating that phosphate's effect on V is not the result of a decrease in the number of myosin molecules actively contributing to actin sliding.

DISCUSSION

We have previously shown that, at low [ATP] ($<\sim$100 μM), actin-sliding velocities, V, follow the [ATP] dependence of $1/\tau_{on}$ (*26*); however, above this critical [ATP], V exceeded the detachment limit by more than a factor of 2 (Figure 2). To determine the biochemical basis for this change in the ATP dependence of actin-sliding velocities, we studied the effects of temperature and inorganic phosphate, P_i, on V both above and below the critical [ATP]. Both temperature and $[P_i]$ affect V differently at low and high [ATP] (Figures 4 and 5), indicating that the biochemistry of actin movement changes at the critical [ATP]. The differential effect of $[P_i]$ is of particular interest. At high [ATP], V is insensitive to $[P_i]$, whereas at low [ATP] V is $[P_i]$-dependent.

The P_i dependence of V at low [ATP] has been previously reported; however, the data presented in this paper imply a new interpretation for this effect, providing new insights into the mechanism for actin sliding at physiological ATP concentrations. Figure 6 shows that, at low [ATP], actin-sliding velocities decrease logarithmically with $[P_i]$, much like active isometric muscle force (*34*, *38*). Analogous to most models of the P_i dependence of muscle force, the P_i dependence of V implies that phosphate affects V through its ln $[P_i]$ contribution to the free energy for myosin's working step, ΔG (*33*). Thus in contrast to the detachment-limited model ($V = d/\tau_{on}$), which assumes detachment kinetics ($1/\tau_{on}$) is the sole biochemical determinant of V, our data indicate that at low [ATP] the biochemistry of myosin's weak-to-strong binding transition also contributes to V.

One interpretation for the ln $[P_i]$ effect, which might make it consistent with the detachment-limited model, is that P_i through mass action induces a net reversal of the weak-to-strong binding transition, reducing the duty ratio to a point where the myosin density is subsaturating for velocity. However, Figure 7 demonstrates that this is not the case, showing that the myosin densities used in these studies are well above saturating levels both in the presence and in the absence of added P_i. In fact, the half-saturation points for V are similar both with and without added P_i, indicating that P_i has little effect on the duty ratio, as previously reported for isometric muscle (*21*).

At low [ATP], there appears to be a strong correlation between ΔG, V, and isometric muscle force, F_0. Although this relationship is difficult to reconcile with most current muscle models, the proportionality of V and F_0 was,

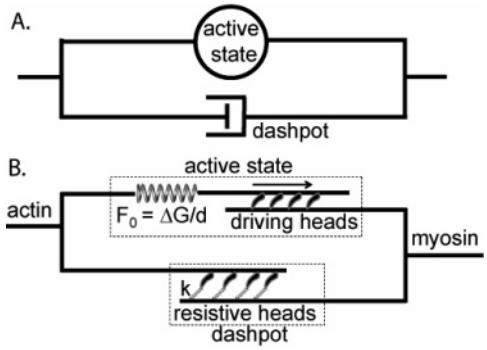

FIGURE 8: Hill's contractile component and a proposal for its molecular basis. (A) Hill used a mechanical circuit to describe muscle's contractile component in terms of an active state, which generates force, in parallel with a damping element. According to this model, actin-shortening velocities, *V*, vary with the force generated in the active state, and thus this model is consistent with our observed relationship between *V*, F_0, and ln [P_i]. (B) Our proposed molecular basis for Hill's contractile component consists of overlapping actin (left) and myosin (right) filaments. In the active state, the force-generating population of myosin heads (upper right) generates a force, F_0, in a macroscopic spring, which both theoretically and experimentally has been shown to be equal to $\Delta G/d$, where ΔG is the free energy for myosin's working step and *d* is the myosin step size. The population of myosin heads that resist actin movement (lower right) is analogous to the damping element in Hill's contractile component.

remarkably, predicted by Hill in 1922 (*39*). Hill argued that stimulation always causes a muscle to generate its maximal force, F_0, and that when muscle is allowed to shorten, part of this force is dissipated through a resistive viscous drag. To describe this phenomenon, he proposed the contractile component model, which consists of a force generator (active state) in parallel with a dashpot element (Figure 8A). According to this model *V* is proportional to F_0, where the proportionality constant is the frictional coefficient of the dashpot.

Hill knew that the lack of a molecular foundation for his model was a problem, but he also recognized that when the chemical basis for muscle contraction was eventually established, the molecular mechanisms for the contractile component would be understood (*24*). In 1999, based on direct observations of mechanochemical coupling in active isometric muscle, we proposed a molecular basis for Hill's active state (*21*, *22*). Briefly, our model assumes that myosin molecules collectively generate a macroscopic force, *F*, in muscle, which is represented in Figure 8B with a macroscopic spring. According to this model, myosin molecules can collectively generate force as long as the total free energy available for work, $\Delta G - Fd$, remains less than zero. When $\Delta G = Fd$, the actin−myosin system reaches a stall, or isometric, force, $F_0 = \Delta G/d$. Thus this model formally links ΔG with *V* and F_0, which is the relationship experimentally demonstrated in this paper.

Here we propose a molecular model for Hill's damping element. In general, the molecular basis for viscous damping between two surfaces is elegantly described by Howard (*20*) in terms of molecular cross-bridges that dissociate at a rate $1/\tau_{on}$. If a force, *F*, is applied parallel to one of these surfaces, the surfaces slide relative to one another at a velocity $V = F/nk\tau_{on}$, where *n* is the total number of cross-bridges and *k* is the cross-bridge stiffness. According to this model (Figure 8B), actin-sliding velocities, *V*, vary proportionally with the internal macroscopic force generated by the driving population (active state) of *n* moles of myosin heads, nF_0, or $V = F_0/k\tau_{on}$. This mechanical description of *V* can be made consistent with the energetic description of *V* developed in eq 1 by setting $F_{resuni} = kd$. As shown in Figure 6, this model accurately describes the relationship between F_0, *V*, and τ_{on} observed at low [ATP]. Interestingly, this model also implies that actin-sliding velocities vary with the compliance, *k*, of actin−myosin linkages.

What does our low [ATP] data and the above analysis tell us about the P_i-independent hypermotile state observed at high [ATP]? In solution kinetics studies, the actin−myosin weak-to-strong binding transition is not easily reversed by P_i due to myosin's relatively high affinity for actin. In fact, only in mechanically loaded systems, such as in isometric muscle (*33*, *38*) or in a laser trap (*26*, *40*), has this transition been shown to be reversible. This is presumably because under high mechanical loads, myosin's working step generates force, allowing the free energy for this transition, ΔG, to be reversibly transferred to mechanical strain. The observation that *V* becomes P_i-independent above the critical [ATP] indicates that the internal forces are dissipated at high [ATP] and ΔG is irretrievably lost as heat through actin movement. We suggest that at high [ATP] ΔG is dissipated through either the shear thinning of strongly bound myosin heads or the work performed on the resistive population of myosin heads in accelerating their ADP release rates. According to a shear thinning model, when [ATP] is increased, fewer myosin heads remain strongly bound to actin. Above the critical ATP concentration, the number of actin-attached myosin heads becomes so low that shear forces generated by the force-generating population of myosin heads (active state) begin to forcibly detach the resistive population of myosin heads (dashpot), as previously proposed by Cooke and co-workers (*41*). This forced detachment of myosin results in a τ_{on} that is shorter than that dictated by ATP-dependent detachment kinetics, resulting in an accelerated *V*. According to a model for the acceleration of the ADP release rate, when [ATP] is increased, the fraction of the resistive myosin heads in the A·M·D state increases as the fraction of rigor heads decreases. We argue that, as proposed for smooth muscle myosin and nonmuscle myosins, the force generated by the working population of myosin (active state) accelerates ADP release from the resistive population of myosin heads in the A·M·D state (*31*, *42*, *43*).

This paper provides the first direct evidence that the biochemistry of the weak-to-strong actin−myosin binding transition, or working step, influences actin-sliding velocities, *V*. The data presented demonstrate that *V* varies with the free energy, ΔG, for the working step at low [ATP], whereas at high [ATP] ΔG contributes to *V* by being used to disrupt bonds or accelerate ADP release kinetics. The implications are significant. Changes in *V* are typically interpreted in terms of changes in *d* or τ_{on}. Our data imply that *V* is also influenced by the kinetics and energetics of myosin's weak-to-strong binding transition.

A model in which *V* is influenced by the biochemistry of the weak-to-strong binding transition might account for observations of proportional changes in *V* and weak-to-strong binding kinetics without a corresponding change in detachment kinetics. For example, point mutations in cardiac actin show reduced sliding velocities and lower average force with no significant change in detachment kinetics when compared

to wild-type cardiac actin (*44*). In their study, Bookwalter et al. propose that a lower average force per actin-bound myosin might lead to the reduction in force and velocity. Similarly, certain mutations in smooth muscle myosin's actin binding loop (loop 2) result in decreased actin-sliding velocities without corresponding changes in detachment kinetics (*45*), indicating a link between the biochemistry of the weak-to-strong binding transition and *V*. In addition to genetic studies, our proposed link between actin−myosin binding kinetics and *V* might also contribute to the observed effects of myosin inhibitors and regulatory proteins on actin-sliding velocities. For instance, reconstitution of actin thin filaments with the regulatory proteins troponin and tropomyosin in the absence of calcium results in a significant decrease in both the rate of actin−myosin binding and actin-sliding velocities, yet has little effect on the actin−myosin detachment rate (*46*). Similarly, reconstitution of thin filaments with troponin and tropomyosin in the presence of calcium results in a 2-fold increase in actin-sliding velocities (*47*) with no established effect on detachment kinetics. Finally, the myosin inhibitor BDM has a significant effect on weak-to-strong binding kinetics (*48*), muscle force (*49*), and *V* (*50*) without a corresponding change in actin−myosin detachment kinetics. Our proposal that the weak-to-strong binding kinetics influences *V* might help us to better understand the effects of these regulatory proteins, disease-related mutations, and inhibitors on actin-sliding velocities.

ACKNOWLEDGMENT

We thank Peter Bayguinov for help with image analysis, Ken Klingler for help with experiments, and Christine Cremo, Kevin Facemyer, Bill Gerthoffer, and Maria Valencik for helpful discussions.

REFERENCES

1. Lymn, R. W., and Taylor, E. W. (1971) Mechanism of adenosine triphosphate hydrolysis by actomyosin, *Biochemistry 10*, 4617−4624.
2. Goldman, Y. E. (1987) Kinetics of the actomyosin ATPase in muscle fibers, *Annu. Rev. Physiol. 49*, 637−654.
3. Cooke, R. (1997) Actomyosin interaction in striated muscle, *Physiol. Rev. 77*, 671−697.
4. Sellers, J. R. (1999) *Myosins*, 2nd ed., Oxford University Press, Oxford, U.K.
5. Molloy, J. E., Burns, J. E., Kendrick-Jones, J., Tregear, R. T., and White, D. C. (1995) Movement and force produced by a single myosin head, *Nature 378*, 209−212.
6. Finer, J. T., Simmons, R. M., and Spudich, J. A. (1994) Single myosin molecule mechanics: piconewton forces and nanometre steps, *Nature 368*, 113−119.
7. Guilford, W. H., Dupuis, D. E., Kennedy, G., Wu, J., Patlak, J. B., and Warshaw, D. M. (1997) Smooth muscle and skeletal muscle myosins produce similar unitary forces and displacements in the laser trap, *Biophys. J. 72*, 1006−1021.
8. Baker, J. E., Brust-Mascher, I., Ramachandran, S., LaConte, L. E., and Thomas, D. D. (1998) A large and distinct rotation of the myosin light chain domain occurs upon muscle contraction, *Proc. Natl. Acad. Sci. U.S.A. 95*, 2944−2949.
9. Reedy, M. K., Holmes, K. C., and Tregear, R. T. (1965) Induced changes in orientation of the cross-bridges of glycerinated insect flight muscle, *Nature 207*, 1276−1280.
10. Huxley, H. E. (1969) The mechanism of muscular contraction, *Science 164*, 1356−1365.
11. Eisenberg, E., and Hill, T. L. (1985) Muscle contraction and free energy transduction in biological systems, *Science 227*, 999−1006.
12. Kron, S. J., and Spudich, J. A. (1986) Fluorescent actin filaments move on myosin fixed to a glass surface, *Proc. Natl. Acad. Sci. U.S.A. 83*, 6272−6276.
13. Harada, Y., Noguchi, A., Kishino, A., and Yanagida, T. (1987) Sliding movement of single actin filaments on one-headed myosin filaments, *Nature 326*, 805−808.
14. Siemankowski, R. F., and White, H. D. (1984) Kinetics of the interaction between actin, ADP, and cardiac myosin-S1, *J. Biol. Chem. 259*, 5045−5053.
15. Siemankowski, R. F., Wiseman, M. O., and White, H. D. (1985) ADP dissociation from actomyosin subfragment 1 is sufficiently slow to limit the unloaded shortening velocity in vertebrate muscle, *Proc. Natl. Acad. Sci. U.S.A. 82*, 658−662.
16. Nyitrai, M., Rossi, R., Adamek, N., Pellegrino, M. A., Bottinelli, R., and Geeves, M. A. (2006) What limits the velocity of fast-skeletal muscle contraction in mammals?, *J. Mol. Biol. 355*, 432−442.
17. Huxley, H. E. (1990) Sliding filaments and molecular motile systems, *J. Biol. Chem. 265*, 8347−8350.
18. Spudich, J. A. (1994) How molecular motors work, *Nature 372*, 515−518.
19. Huxley, A. F. (1957) Muscle structure and theories of contraction, *Prog. Biophys. 7*, 255−315.
20. Howard, J. (2001) *Mechanics of motor proteins and the cytoskeleton*, Sinauer Associates, Sunderland, MA.
21. Baker, J. E., LaConte, L. E., Brust-Mascher, I. I., and Thomas, D. D. (1999) Mechanochemical coupling in spin-labeled, active, isometric muscle, *Biophys. J. 77*, 2657−2664.
22. Baker, J. E., and Thomas, D. D. (2000) A thermodynamic muscle model and a chemical basis for A. V. Hill's muscle equation, *J. Muscle Res. Cell Motil. 21*, 335−344.
23. Baker, J. E. (2004) Free energy transduction in a chemical motor model, *J. Theor. Biol. 228*, 467−476.
24. Hill, A. V. (1938) The heat of shortening and the dynamic constants of muscle, *Proc. R. Soc. London, Ser. B 126*, 136−195.
25. Sweeney, H. L., Rosenfeld, S. S., Brown, F., Faust, L., Smith, J., Xing, J., Stein, L. A., and Sellers, J. R. (1998) Kinetic tuning of myosin via a flexible loop adjacent to the nucleotide binding pocket, *J. Biol. Chem. 273*, 6262−6270.
26. Baker, J. E., Brosseau, C., Joel, P. B., and Warshaw, D. M. (2002) The biochemical kinetics underlying actin movement generated by one and many skeletal muscle myosin molecules, *Biophys. J. 82*, 2134−2147.
27. Warshaw, D. M., Desrosiers, J. M., Work, S. S., and Trybus, K. M. (1990) Smooth muscle myosin cross-bridge interactions modulate actin filament sliding velocity in vitro, *J. Cell Biol. 111*, 453−463.
28. Pardee, J. D., and Spudich, J. A. (1982) Purification of muscle actin, *Methods Enzymol. 85* (Part B), 164−181.
29. Fabiato, A., and Fabiato, F. (1979) Calculator programs for computing the composition of the solutions containing multiple metals and ligands used for experiments in skinned muscle cells, *J. Physiol. (Paris) 75*, 463−505.
30. Linari, M., Brunello, E., Reconditi, M., Sun, Y. B., Panine, P., Narayanan, T., Piazzesi, G., Lombardi, V., and Irving, M. (2005) The structural basis of the increase in isometric force production with temperature in frog skeletal muscle, *J. Physiol. 567*, 459−469.
31. Baker, J. E., Brosseau, C., Fagnant, P., and Warshaw, D. M. (2003) The unique properties of tonic smooth muscle emerge from intrinsic as well as intermolecular behaviors of myosin molecules, *J. Biol. Chem. 278*, 28533−28539.
32. Tyska, M. J., Dupuis, D. E., Guilford, W. H., Patlak, J. B., Waller, G. S., Trybus, K. M., Warshaw, D. M., and Lowey, S. (1999) Two heads of myosin are better than one for generating force and motion, *Proc. Natl. Acad. Sci. U.S.A. 96*, 4402−4407.
33. Cooke, R., and Pate, E. (1985) The effects of ADP and phosphate on the contraction of muscle fibers, *Biophys. J. 48*, 789−798.
34. Pate, E., and Cooke, R. (1989) Addition of phosphate to active muscle fibers probes actomyosin states within the powerstroke, *Pfluegers Arch. 414*, 73−81.
35. Warshaw, D. M., Desrosiers, J. M., Work, S. S., and Trybus, K. M. (1991) Effects of MgATP, MgADP, and P_i on actin movement by smooth muscle myosin, *J. Biol. Chem. 266*, 24339−24343.
36. Uyeda, T. Q., Kron, S. J., and Spudich, J. A. (1990) Myosin step size. Estimation from slow sliding movement of actin over low densities of heavy meromyosin, *J. Mol. Biol. 214*, 699−710.
37. Harris, D. E., and Warshaw, D. M. (1993) Smooth and skeletal muscle myosin both exhibit low duty cycles at zero load in vitro, *J. Biol. Chem. 268*, 14764−14768.

38. Dantzig, J. A., Goldman, Y. E., Millar, N. C., Lacktis, J., and Homsher, E. (1992) Reversal of the cross-bridge force-generating transition by photogeneration of phosphate in rabbit psoas muscle fibres, *J. Physiol. 451*, 247−278.
39. Hill, A. V. (1922) The maximum work and mechanical efficiency of human muscles, and their most economical speed, *J. Physiol. 56*, 19−41.
40. Takagi, Y., Homsher, E. E., Goldman, Y. E., and Shuman, H. (2006) Force generation in single conventional actomyosin complexes under high dynamic load, *Biophys. J. 90*, 1295−1307.
41. Cooke, R., White, H., and Pate, E. (1994) A model of the release of myosin heads from actin in rapidly contracting muscle fibers, *Biophys. J. 66*, 778−788.
42. Cremo, C. R., and Geeves, M. A. (1998) Interaction of actin and ADP with the head domain of smooth muscle myosin: implications for strain-dependent ADP release in smooth muscle, *Biochemistry 37*, 1969−1978.
43. Baker, J. E., Krementsova, E. B., Kennedy, G. G., Armstrong, A., Trybus, K. M., and Warshaw, D. M. (2004) Myosin V processivity: multiple kinetic pathways for head-to-head coordination, *Proc. Natl. Acad. Sci. U.S.A. 101*, 5542−5546.
44. Bookwalter, C. S., and Trybus, K. M. (2006) Functional consequences of a mutation in an expressed human alpha-cardiac actin at a site implicated in familial hypertrophic cardiomyopathy, *J. Biol. Chem. 281*, 16777−16784.
45. Joel, P. B., Trybus, K. M., and Sweeney, H. L. (2001) Two conserved lysines at the 50/20-kDa junction of myosin are necessary for triggering actin activation, *J. Biol. Chem. 276*, 2998−3003.
46. Kad, N. M., Kim, S., Warshaw, D. M., VanBuren, P., and Baker, J. E. (2005) Single-myosin crossbridge interactions with actin filaments regulated by troponin-tropomyosin, *Proc. Natl. Acad. Sci. U.S.A. 102*, 16990−16995.
47. Homsher, E., Nili, M., Chen, I. Y., and Tobacman, L. S. (2003) Regulatory proteins alter nucleotide binding to acto-myosin of sliding filaments in motility assays, *Biophys. J. 85*, 1046−1052.
48. Herrmann, C., Wray, J., Travers, F., and Barman, T. (1992) Effect of 2,3-butanedione monoxime on myosin and myofibrillar ATPases. An example of an uncompetitive inhibitor, *Biochemistry 31*, 12227−12232.
49. Zhao, L., Naber, N., and Cooke, R. (1995) Muscle cross-bridges bound to actin are disordered in the presence of 2,3-butanedione monoxime, *Biophys. J. 68*, 1980−1990.
50. Regnier, M., Chase, P. B., and Martyn, D. A. (1999) Contractile properties of rabbit psoas muscle fibres inhibited by beryllium fluoride, *J. Muscle Res. Cell Motil. 20*, 425−432.

BI0614840